IOPscience iopscience.iop.org

Home Search Collections Journals About Contact us My IOPscience

Steady-state and small signal analysis of terahertz ballistic tunnel transit-time oscillator

This article has been downloaded from IOPscience. Please scroll down to see the full text article.

2004 J. Phys.: Condens. Matter 16 627

(http://iopscience.iop.org/0953-8984/16/4/011)

View the table of contents for this issue, or go to the journal homepage for more

Download details:
IP Address: 129.252.86.83
The article was downloaded on 28/05/2010 at 07:18

Please note that terms and conditions apply.

INSTITUTE OF PHYSICS PUBLISHING JOURNAL OF PHYSICS: CONDENSED MATTER

J. Phys.: Condens. Matter **16** (2004) 627–634 PII: S0953-8984(04)71724-5

Steady-state and small signal analysis of terahertz ballistic tunnel transit-time oscillator

J T Lü and J C Cao

State Key Laboratory of Functional Materials for Informatics, Shanghai Institute of Microsystem and Information Technology, Chinese Academy of Sciences, 865 Changning Road, Shanghai 200050, People's Republic of China

Received 9 November 2003
Published 16 January 2004
Online at stacks.iop.org/JPhysCM/16/627 (DOI: 10.1088/0953-8984/16/4/011)

Abstract
We have considered an InGaAs/InAlAs/InP/InGaAs ballistic tunnel transit-time oscillator under dc and small high frequency ac electric field. Using the quantum transmitting boundary method coupled with the Poisson equation, we have studied electron tunnelling through the barrier assuming that the electrons have a nonparabolic dispersion, and have got the steady state field–current characteristics (E–j) of the oscillator. As a result of the small signal analysis based on these characteristics, we find the negative resistance windows, which are the work regions of the oscillator. The windows get much deeper with the increase of the dc electric field. Their frequencies are in the terahertz (THz) range, which may be used to develop efficient and powerful sources of this range.

1. Introduction

In 1958, the tunnel injection transit-time (TUNNETT) diode was proposed by Nishizawa and Watanabe [1]. The concept of this diode was introduced in the analysis of the high-frequency properties of the avalanching negative resistance diode which is today called the IMPATT diode. Now TUNNETT diodes are considered to have better noise and frequency performance than IMPATT diodes due to the fundamental properties of tunnelling [2]. Their better performance allows them to serve as millimetre and submillimetre wave sources up to the terahertz (THz) range [3]. Sources and detectors in this range have aroused considerable interest in the past few years [3–10]. With the advances in MBE techniques, many TUNNETT diodes have been realized [11–13]. Recently, Gribnikov *et al* [14] proposed a new type of ballistic TUNNETT oscillator for the terahertz range and analysed the linear response of the oscillator under small high frequency ac electric field. They also left some additional problems that need to be addressed, which include the field–current (E–j) characteristics of the oscillator. The field here is the electric field across the tunnel barrier.

In this paper we report on numerical studies of the E–j characteristics of one version of the TUNNETT oscillator. The structure of the TUNNETT oscillator is illustrated in figure 1 of [14].

 © 2004 IOP Publishing Ltd Printed in the UK

Due to the total length of the oscillator, we use the quantum transmitting boundary method (QTBM) to simulate electron tunnelling in the oscillator. QTBM was originally developed by Lent and Kirkner [15] for treating electron waveguides, and was adapted by Frensley [16] to treat heterostructure tunnel devices. It is robust and numerically stable compared to an alternative method used in electron tunnelling, which is called the transfer matrix method (TMM) [17]. The calculated results indicated that the selection of the tunnel barrier and the length of the transit space can increase the work regions of the TUNNETT oscillator into the terahertz range.

The organization of this paper is as follows. In section 2 we discuss in detail the application of QTBM in solving the Schrödinger equation with semi-infinite boundary conditions. In section 3 we show how to get the tunnelling current self-consistently in TUNNETT diodes when the electrons have nonparabolic dispersion. In section 4 we apply the tunnelling model to the TUNNETT oscillator. Finally, in section 5 we give the conclusion of this paper.

2. Tunnelling model

As a widely used electron injection mechanism in many electronic devices, electron tunnelling across arbitrary potential barriers has been studied using different models. One of the most important physical parameters in treating tunnelling is the quantum transmission coefficient (QTC), which is in general related to the energy of electrons. To obtain QTC, the WKB or Gundlach method [18] can be used when the barrier shape is triangular or trapezoidal. But energy barriers which are not of triangular or trapezoidal shape are not treated correctly by these models. To accurately describe tunnelling in such cases, the Schrödinger equation must be solved. This can be achieved by using the TMM or QTBM.

In our TUNNETT oscillator, electrons in the cathode pool can tunnel across the barrier and inject into the transit space. They are finally absorbed by the anode contact without any reflection or back-scattering. This process can be simulated as electrons in the cathode tunnelling across the barrier and transit space into the anode, which can be described by the simplest Hermitian effective-mass Schrödinger equation:

$$-\frac{\hbar^2}{2}\frac{\partial}{\partial x}\left(\frac{1}{m(x)}\frac{\partial}{\partial x}\psi(x)\right)+V(x)\psi(x)=E\psi(x), \tag{1}$$

where $V(x)$ includes both band-edge discontinuities and macroscopic electric fields, $m(x)$ is the space dependent effective mass, $\psi(x)$ is the wavefunction, and E represents energy. We use the finite difference method to discretize equation (1) and obtain

$$H_{\sigma,\sigma-1}F_{\sigma-1}+\bar{H}_{\sigma,\sigma}F_{\sigma}+H_{\sigma,\sigma+1}F_{\sigma+1}=0, \tag{2}$$

where $\bar{H}\equiv(H-E)$, and

$$H_{\sigma,\sigma-1}F_{\sigma\pm1}=-\frac{\hbar^2}{d^2}\left(\frac{1}{m_\sigma+m_{\sigma\pm1}}\right), \tag{3}$$

$$H_{\sigma,\sigma}=V_\sigma-H_{\sigma,\sigma-1}-H_{\sigma,\sigma+1}, \tag{4}$$

with d being the discretization length, and σ being the discretization index $(1<\sigma<N)$.

We can employ the QTBM to describe the boundary conditions for the semi-infinite boundary regions on the cathode and anode contacts, where the potential $V(x)$ is constant. For a given energy E, the general solution to the Schrödinger equation $\psi(x)$ in these regions can be written as

$$\psi(x)=\begin{cases}a_{\mathrm{c}}\mathrm{e}^{\mathrm{i}k_{\mathrm{c}}x}+b_{\mathrm{c}}\mathrm{e}^{-\mathrm{i}k_{\mathrm{c}}x}, & \text{at cathode}\\ a_{\mathrm{a}}\mathrm{e}^{-\mathrm{i}k_{\mathrm{a}}x}+b_{\mathrm{a}}\mathrm{e}^{\mathrm{i}k_{\mathrm{a}}x}, & \text{at anode}\end{cases} \tag{5}$$

where a_c and a_a are the amplitudes of the incoming wave components, b_c and b_a are the amplitudes of the outgoing wave components, and k_c and k_a are the wavenumbers of the cathode and anode region, respectively. We assume that the simulated region is discretized into N meshpoints, and that meshpoints 1 and 2 ($N-1$ and N) are in the cathode (anode) semi-infinite flat-band region. From equation (5) we get

$$\psi(1) - e^{ik_c d}\psi(2) = a_c(1 - e^{2ik_c d}), \tag{6}$$

$$\psi(N) - e^{ik_a d}\psi(N-1) = a_a(1 - e^{2ik_a d}). \tag{7}$$

The two boundary conditions, together with the differential Schrödinger equation, constitute a tridiagonal system of N linear equations with N unknowns $\psi(1), \psi(2), \ldots, \psi(N)$, which can be solved with readily available numerical routines. The QTC is given by

$$T_c = \frac{k_a}{k_c}\frac{m_c}{m_a}|\psi(N-1)|^2, \tag{8}$$

where m_c and m_a are the effective masses of electrons in the cathode and anode regions.

3. E–j calculation with nonparabolic dispersion

To obtain the current density from the QTC, the commonly used expression in the literature is based on the work of Tsu and Esaki [19]. It is applicable for electrons with parabolic dispersion in the transverse directions. But here the electrons have a nonparabolic dispersion as [14]

$$\varepsilon(p) = V_S\left(\sqrt{p_S^2 + p^2} - p_S\right), \tag{9}$$

where V_S is the saturated electron velocity and $p_S = mV_S$. To calculate the E–j characteristics, we need the expressions of the current density and carrier concentration corresponding to this specific nonparabolic dispersion.

In general, to obtain the density of the observable we should first calculate the expectation value of the observable quantity for each state, taking the scattering states to be normalized to unit amplitude. The integral of the expectation value multiplied by the electron distribution for all states gives us the density of the observable. The expectation value of the density for a state φ is simply

$$n_\varphi(x) = \varphi^\star(x)\varphi(x). \tag{10}$$

The expectation value of J is

$$\langle\varphi|J|\varphi\rangle = q\upsilon T_c, \tag{11}$$

where υ is the group velocity. Due to the inherent difficulties involved with normalizing a wavefunction that does not correspond to a quasi-bound state [20, 21], we have chosen a normalization such that the resulting total electron density in the structure exactly compensates the net positive charge. Once the solution has converged, the quantum-mechanical electron density at the border of the electrode always ends up to be equal to the semiclassical value there, provided that the borders are chosen sufficiently far away from the barrier.

The expression for the total current density J can be written as

$$J = q\int_0^\infty \frac{dE_\parallel}{2\pi\hbar} T_c(E_\parallel)(F(E_\parallel - E_{f,c}) - F(E_\parallel - E_{f,a})), \tag{12}$$

where

$$F(E) = \frac{mk_B T}{\pi\hbar^2\beta}\ln(1 + e^{-\frac{E}{k_B T}}) + \frac{1}{\pi\hbar^2 V_S^2}\int \frac{E_\perp}{1 + e^{\frac{E+E_\perp}{k_B T}}} dE_\perp, \tag{13}$$

$E_{f,c}$ and $E_{f,a}$ denote the Fermi levels of the cathode and anode region, respectively, m denotes the electron effective mass, T is the absolute temperature, k_B the Boltzmann constant, and $E_\perp$ and $E_\parallel$ are the electron energy perpendicular and parallel to the current direction, respectively.

Similarly, we can get the carrier concentration

$$n = \int_0^\infty \frac{(F'(E_\parallel - E_{f,c}) + F'(E_\parallel - E_{f,a}))}{2\pi\hbar V_S} \, dE_\parallel, \tag{14}$$

where

$$F'(E) = \frac{1}{\pi\hbar^2 V_S^2} \int \frac{(E_\perp + mV_S^2)(E_\perp + mV_S^2 + E)}{\sqrt{(E_\perp + E)^2 + 2mV_S^2(E_\perp + E)}} \frac{1}{1 + e^{\frac{E+E_\perp}{k_B T}}} \, dE_\perp. \tag{15}$$

The model we use here does not allow the inclusion of scattering of carriers. However, in most real devices, scattering plays an important role in producing the self-consistent energy bands and resulting device operation. The semi-classical model inherently includes scattering. A simple compromise is to use the semi-classical model in the electrode regions and the quantum model in other regions, though the semi-classical model ignores all the quantum effects in the calculation of carrier profile:

$$n = 2 \int \frac{d^3k}{(2\pi)^3} f(E(k)), \tag{16}$$

where f is the Fermi–Dirac distribution function.

To get a self-consistent solution, the Poisson equation needs to be coupled with the above linear system. We can use the Gummel method to get a self-consistent solution of the wavefunction and then other values of interest.

4. Application to TUNNETT oscillator

Our TUNNETT oscillator is configured as follows. The transit space is undoped InP, the cathode and the anode contact $In_{0.53}Ga_{0.47}As$ alloy, and the tunnel barrier is the $In_{0.52}Al_{0.48}As$ alloy. The cathode and anode concentrations are 3.5×10^{18} cm^{-3}. The conduction band offset between the cathode and the barrier, and the barrier and the transit space are 0.52 and 0.30 eV, respectively. The electron effective mass is 0.04 m_0 at the cathode, 0.077 m_0 at the barrier, and 0.08 m_0 at the transit space. The Fermi levels are determined according to [23]. Other parameters are taken from [14]: $V_S = 1.3 \times 10^8$ cm s^{-1}, $l = 70$ nm. The temperature we used in the calculation is room temperature $T = 300$ K.

We show the potential distribution (right-hand axis) and the carrier density profile (left-hand axis) obtained from the proposed self-consistent model in figure 1. The bias voltage is 0.75 V. As we can see, the potential does not drop linearly from the anode to the cathode. There forms an accumulation layer at the anode region, and correspondingly, a depletion layer at the cathode. These are due to the bound states of the barrier, as we can see from other similar structures [22, 24]. As stated in section 3, we use the semi-classical expressions of the carrier concentration, so we do not have the Friedel oscillations in the electrode regions that will appear if we use the quantum-mechanical expressions. The carrier concentration in the barrier and the transit space is much smaller than that in the electrode regions due to the relatively long transit space. The inset shows a relatively clear picture of the carrier profile in the barrier region, which is too small in magnitude to be seen in the main figure.

The QTC $T_c(E)$ across the TUNNETT oscillator is calculated using above parameters, and shown in figure 2. The oscillatory behaviour of $T_c(E)$ is due to resonance through the bound states above the barrier. It can be seen that there are various resonances in the structure.

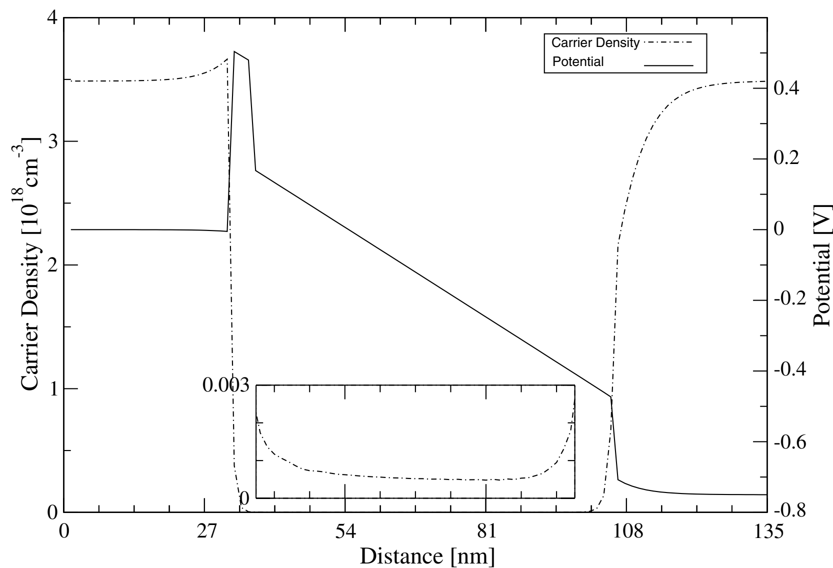

Figure 1. Carrier density and potential profile of the TUNNETT oscillator when the biased voltage is 0.75 V. The transit space length is $l = 70$ nm and undoped, the barrier width is $b = 5$ nm, the barrier height is 0.52 eV, the electrode concentration is $n = 3.5 \times 10^{18}$ cm^{-3} and the temperature is 300 K. The inset shows the carrier profile in the barrier region, which is too small in magnitude to be seen in the main figure. The tick labels of the inset are the same as in the main figure and are omitted.

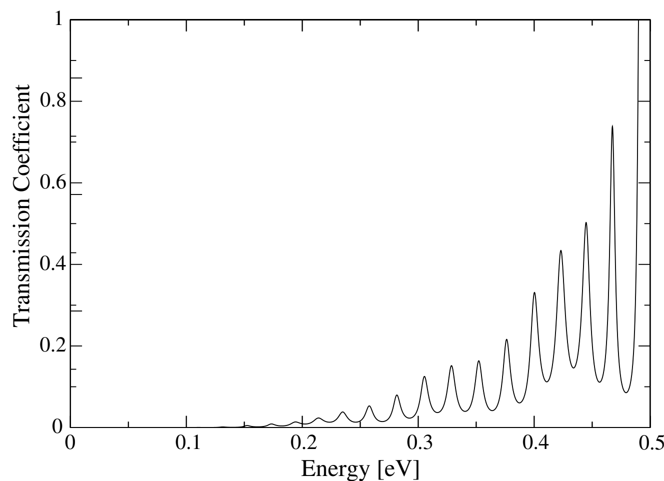

Figure 2. The TC of electrons as a function of energy when the oscillator is biased at 0.75 V. The other parameters are the same as in figure 1.

These resonances are of importance for the accuracy of the total current and must be resolved appropriately. The number and steepness of the peaks depend on the number and width of the barriers, as well as on the applied voltage. The oscillator has only one barrier, so we do not have strong resonant states as we see in the resonant tunnelling diode. According to the QTC of electrons, we can get the tunnel current using equation (12). The E–j characteristics

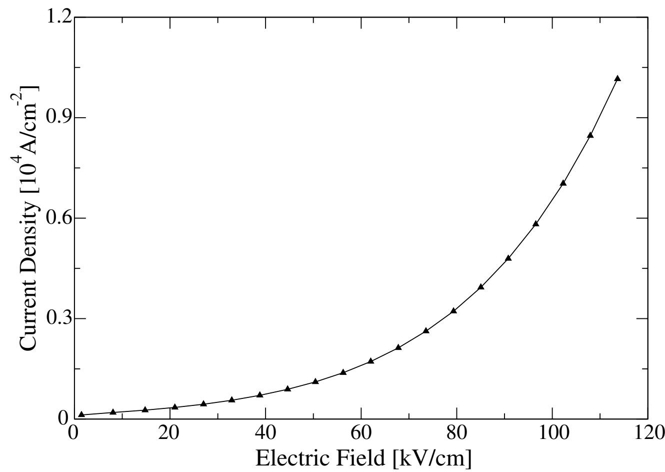

Figure 3. E–j characteristics of the ballistic TUNNETT oscillator. The other parameters are the same as in figure 1.

are shown in figure 3. The current increases almost linearly at low electric field and more sharply at higher electric field. This is due to the increase of transmission coefficient when the electric field gets larger. No negative differential resistance regions appear, since we have only one long barrier in the oscillator. Compared to the interband tunnelling injection of electrons, tunnelling through a heterobarrier is more efficient. We can get the same current density with about ten times smaller electric field [14].

Now we can obtain the values of $A_0 = eE(j)(\kappa_D/2ejmV_S)^{1/2}$ and $\Omega_0 = \mathrm{d}j/\mathrm{d}E(mV_S/2ej\kappa_D)^{1/2}$ from the current j. These two parameters represent the finite resistance of the tunnel emitter controlled by an electric field applied to it. For the space-charge limited case when the tunnel emitter barrier does not limit electron injection from the electrode, $A_0 = 0$ and $\Omega_0 = \infty$ [14]. But [14] did not investigate their interrelations and considered them as self-consistent independent parameters. After that we computed the conductance of the TUNNETT oscillator biased by a dc and high frequency ac electric field using the small-signal approximation proposed in [14], which is shown in figure 4. Due to the influence of the nonparabolicity of the electron dispersion on the negative windows [14], we use the more realistic nonparabolic dispersion equation (9) in our simulation. From figure 4 we can see that two obvious dynamic negative resistance windows in the terahertz range are clearly shown under each current density despite the influence of the electron dispersion nonparabolicity. The first negative window seems to have more attractive potential of application [25, 26]. Since the electron tunnelling time is much shorter than the transit time, according to the operation principle of a transit-time diode, we can change the length of the transit space or use different material to control the negative window frequencies. We can also see that the windows get much deeper with increasing current density. This is what we prefer in the potential use of a terahertz oscillator.

5. Conclusion

We have simulated in this paper one specific version of the ballistic TUNNETT oscillator proposed in [14], which is considered as a possible oscillator for the terahertz range. One of the additional problems left in [14], the E–j characteristics of the oscillator, has been studied

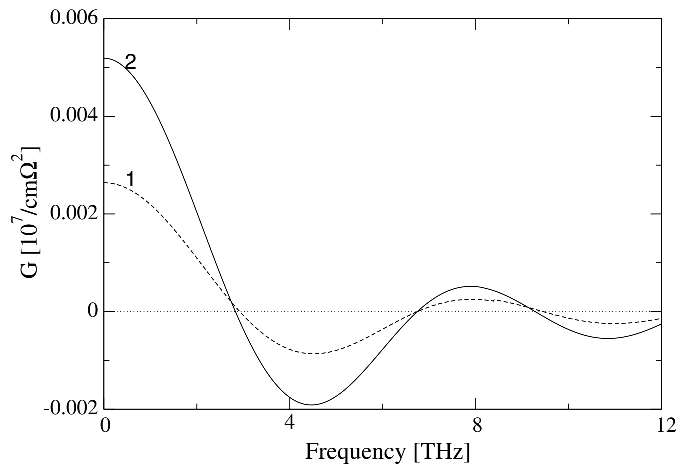

Figure 4. Conductance G of the TUNNETT oscillator plotted against frequency f at the current density $j = 0.48 \times 10^4$ A cm^{-2} (1), $j = 0.85 \times 10^4$ A cm^{-2} (2). The other parameters are the same as those in figure 1.

numerically. The calculated results indicate that heterobarrier tunnelling has more attractive advantage in electron injection than interband tunnelling. We have also obtained the negative conductance windows of the TUNNETT oscillator. We need to do some transit time simulation of this oscillator in the future.

Acknowledgments

This work was supported by the National Natural Science Foundation of China (10390162, 60136010), the Special Funds for Major State Basic Research Project (2001CCA02800G and 20000683), and the Funds from the Shanghai Municipal Commisions of Science and Technology of China (011661075, 03JC14082). The authors would like to thank Y H Zhang, B H Wu and S W Gao for many helpful discussions.

References

[1] Nishizawa J and Watanabe Y 1958 *Res. Institute Tohoku Univ. Sci. Rep.* **10** 91
[2] Nishizawa J I, Motoya K and Okuno Y 1978 *IEEE Trans. Microw. Theory Tech.* **26** 1029
[3] Haddad G I, East J R and Kidner C 1991 *Microw. Opt. Technol. Lett.* **4** 1
[4] Cao J C and Lei X L 2003 *Phys. Rev.* B **67** 085309
[5] Cao J C, Liu H C and Lei X L 2000 *Phys. Rev.* B **61** 5546
[6] Cao J C, Liu H C and Lei X L 2000 *J. Appl. Phys.* **87** 2867
[7] Gribnikov Z S, Bashirov R R and Mitin V V 2001 *IEEE. J. Sel. Top. Quant.* **7** 630
[8] Köhler R, Tredicucci A, Beltram F, Beere H E, Linfield E H, Davies A G, Ritchie D A, Lotti R C and Rossi F 2002 *Nature* **417** 156
[9] Williams B S, Callebaut H, Kumar S and Hu Q 2003 *Appl. Phys. Lett.* **82** 1015
[10] Tamosiunas V, Zobl R, Ulrich J and Unterrainer K 2003 *Appl. Phys. Lett.* **83** 3873
[11] Kidner C, Eisele H and Haddad G I 1992 *Electron. Lett.* **28** 511
[12] Eisele H and Haddad G I 1995 *IEEE Trans. Microw. Theory Tech.* **43** 210
[13] Bauer T, Rösch M, Claassen M and Harth W 1994 *Electron. Lett.* **30** 1319
[14] Gribnikov Z S, Vagidov N Z, Mitin V V and Haddad G I 2003 *J. Appl. Phys.* **93** 5435
[15] Lent C S and Kirkner D J 1990 *J. Appl. Phys.* **67** 6353
[16] Frensley W R 1992 *Superlatt. Microstruct.* **11** 347

[17] Gehring A, Kosina H, Grasser T and Selberherr S 2003 *4th European Workshop on Ultimate Integration of Silicon* p 131
[18] Shanware A, Shiely J P and Massoud H Z 1999 *IEDM Tech. Dig.* p 815
[19] Tsu R and Esaki L 1973 *Appl. Phys. Lett.* **22** 562
[20] Tan H, Snider G L, Chang L D and Lu E H 1990 *J. Appl. Phys.* **68** 4071
[21] Tabatabaie N *et al* 1988 *Appl. Phys. Lett.* **53** 2528
[22] Biegel B A 1997 Quantum electronic device simulation *PhD Dissertation*
[23] Joyce W B and Dixon R W 1977 *Appl. Phys. Lett.* **31** 354
[24] Ohnishi H, Inata T, Muto S, Yokoyama N and Shibatomi A 1986 *Appl. Phys. Lett.* **49** 1248
[25] Benham W E 1931 *Phil. Mag.* **11** 457
[26] Llewellyn F B and Bowen A E 1939 *Bell Syst. Tech. J.* **18** 280